Toward 3D conical-wave migration in tilted elliptic cylindrical coordinates

Jeff Shragge and Guojian Shan

ABSTRACT

We extend conical-wave migration to tilted elliptic cylindrical (TEC) coordinate systems. When inline coordinate tilt angles are well-matched to the inline plane-wave ray parameters, the TEC coordinate extension affords accurate propagation of steep-dip and turning-wave components of conical wavefields in both the in- and crossline directions. We show that wavefield extrapolation in TEC coordinates is no more complicated than propagation in elliptically anisotropic media. Impulse response tests illustrate the accuracy of the the approach. Future work will apply the conical-wave migration approach to field data sets.

INTRODUCTION

Wave-equation migration (WEM) methods routinely are now used to generate seismic images in areas of complex geology. One common class of WEM approaches is shot-profile migration based on one-way wavefield extrapolation. The first step is to specify source and receiver wavefields that consist of modeled point sources and the recorded shot-profile data, respectively. The second step is to propagate these two wavefields through the velocity model and correlate them to form an image. A drawback of this approach is that individual profiles routinely cover only a small portion of the total survey area and many shot-profile migrations are required to infill the image volume. One way to make this type of WEM more efficient is to migrate a reduced number of composite source and receiver profiles each covering a broader area of the image space; however, this requires mixing the information from different shots and can lead to image crosstalk.

Plane-wave migration (PWM) is one technique for reducing total migration cost by generating a lower number of composite wavefields (**???????**). The key idea is to synthesize a set of composite receiver wavefields that would have been recorded were a planar source wavefield used. One then generates the PWM image by propagating the modeled planar source wavefield and the composite receiver wavefield through the velocity and computing a (weighted) correlation. **?** and **?** demonstrate that PWM is equivalent to shot-profile migration in situations where one uses large numbers of plane waves with well-sampled plane-wave dip spectra. **?** also prove that 3D PWM is equivalent to conical-wave migration of individual sail lines formed as inline composite wavefields. The approach is termed conical-wave because the source wavefronts form

cones for non-zero inline plane-wave ray parameters. More generally, these PWM approaches are examples of phase-encoding class of WEM (**????**).

The migration of plane-wave sections - though more efficient than shot-profile migration - is similarly restricted by one-way wavefield extrapolation assumptions. The most common limitation is a difficulty in propagating waves at steep angles and turning waves by design, both of which are important for accurate imaging in complex geologic areas. **?** circumvent this problem by proposing fully 3D PWM in a suite of tilted Cartesian meshes. This effectively orients the wavefield extrapolation axis toward the plane-wave take-off vector, enabling more accurate bulk propagation of plane-wave energy.

One logistical complication of performing fully 3D PWM is it requires propagating image-space-sized data volumes on a number of meshes tilting in both the in- and crossline directions. This leads to a number of computational issues associated with the significant memory footprint. In this paper, we follow a similar alternative coordinate system approach for performing PWM. However, we chose to concentrate on using a coordinate system well-suited for migrating individual sail lines with a reduced memory footprint. We term this approach conical-wave migration on tilted elliptic cylindrical coordinates.

A 3D elliptic cylindrical coordinate system is formed by concatenating a set of confocal 2D elliptic surfaces along the remaining axis. We orient the invariant and elliptic surfaces in the in- and crossline direction, respectively. We extrapolate the conical wavefields outward on a series of confocal elliptic cylindrical shells. This allows source and receiver wavefields with zero inline dip to overturn, if necessary, in the crossline direction. We also introduce an additional degree of freedom to tilt the coordinate system in the direction of the invariant inline axis. Consequently, we propagate plane-wave sources with non-zero inline dips accurately to steep, and even turning, angles.

We begin by revisiting 3D plane-wave and conical-wave migration theory. We introduce the tilted elliptic cylindrical coordinates and then develop the corresponding wavenumber used to form the wavefield extrapolation operator. We then discuss numerical issues regarding implementing the finite-difference extrapolation scheme, and present the point-source responses.

PLANE-WAVE MIGRATION

The 3D plane-wave and conical-wave migration theory discussed in this paper draws heavily on that in **?**. We restate a number of significant and related points for completeness, though with a slightly different notation.

Performing 3D plane-wave migration is similar in many respects to 3D shot-profile migration. The main difference is rooted in how the complete source and receiver wavefield volumes, $\overline{S}$ and $\overline{R}$, are specified from individual source and receiver records,

S_{ij} and R_{kl}, prior to imaging. The complete wavefields are generated by filtering the source and receiver profiles by a function dependent on the inline and cross-line plane-wave slownesses, $\boldsymbol{p_\xi} = [p_{\xi_1}, p_{\xi_2}]$. The phase-encoded wavefields are then propagated through the migration domain (herein defined by $\boldsymbol{\xi} = [\xi_1, \xi_2, \xi_3]$) to generate the source and receiver wavefield volumes

$$\overline{S(\boldsymbol{\xi}|\omega)} = \sum_{i=1}^{M}\sum_{j=1}^{N} S_{ij}(\boldsymbol{\xi}|\omega) f(\omega) \mathrm{e}^{\mathrm{i}\omega[p_{\xi_1}\Delta\xi_1(i-p)+p_{\xi_2}\Delta\xi_w(j-q)]}, \tag{1}$$

$$\overline{R(\boldsymbol{\xi}|\omega)} = \sum_{k=1}^{M}\sum_{l=1}^{N} R_{kl}(\boldsymbol{\xi}|\omega) f(\omega) \mathrm{e}^{\mathrm{i}\omega[p_{\xi_1}\Delta\xi_1(k-p)+p_{\xi_2}\Delta\xi_2(l-q)]}, \tag{2}$$

where $f(\omega)$ is a frequency (ω) filter to be discussed below, $\Delta\xi_1$ and $\Delta\xi_2$ are the inline and crossline sampling intervals, p and q are reference spatial indices in the inline and crossline directions, i and j are the inline and crossline components fixing the source position, k and l are the inline and crossline components fixing the receiver position, and M and N are the number of inline and cross-line records. Note that the phase-encoding is performed at the surface and is unaffected by the subsequent wavefield extrapolation. Thus, this formulation is valid for any coordinate system, including TEC computational meshes.

The image volume $I(\boldsymbol{\xi})$ is formed from a series of plane-wave migration images, $I^{pw}(\boldsymbol{\xi}|\boldsymbol{p_\xi})$, by correlating the composite plane-wave source and receiver wavefields and summing the result over each frequency. The plane-wave migration kernel mixes energy from a source, $S_{ij}(\boldsymbol{\xi}|\omega)$, and a receiver, $R_{kl}(\boldsymbol{\xi}|\omega)$, wavefield according to

$$\begin{aligned} I(\boldsymbol{\xi}) &= \sum_{p_{\xi_1}}\sum_{p_{\xi_2}}\sum_{i,k=1}^{M}\sum_{j,l=1}^{N} I^{pw}_{ijkl}(\boldsymbol{\xi}|\boldsymbol{p_\xi}) \\ &= \sum_{p_{\xi_1}}\sum_{p_{\xi_2}}\sum_{i,k=1}^{M}\sum_{j,l=1}^{N}\sum_{\omega} |f(\omega)|^2 \, S^*_{ij}(\boldsymbol{\xi}|\omega) \, R_{kl}(\boldsymbol{\xi}|\omega) \mathrm{e}^{\mathrm{i}\omega[p_{\xi_1}\Delta\xi_1(i-k)+p_{\xi_2}\Delta\xi_2(j-l)]}, \end{aligned} \tag{3}$$

where * indicates complex conjugate.

Generally, mixing wavefields of differing S_{ij} and R_{kl} indices introduces crosstalk into the image volume. However, plane-wave migration will be crosstalk-free when the following hold:

$$\begin{aligned} \lim_{N_{p_{\xi_1}}\to\infty} \sum_{\alpha=-N_{p_{\xi_1}}}^{N_{p_{\xi_1}}} \mathrm{e}^{\mathrm{i}\omega\alpha\Delta p_{\xi_1}\Delta\xi_1(i-k)} &= |\omega|^{-1}\delta_{ik}, \\ \lim_{N_{p_{\xi_2}}\to\infty} \sum_{\alpha=-N_{p_{\xi_2}}}^{N_{p_{\xi_2}}} \mathrm{e}^{\mathrm{i}\omega\alpha\Delta p_{\xi_2}\Delta\xi_2(j-l)} &= |\omega|^{-1}\delta_{jl}. \end{aligned} \tag{4}$$

Assuming that equation 4 approximately is valid (i.e., for large values of $N_{p_{\xi_1}}$ and

$N_{p_{\xi_2}}$), we may rewrite equation 3 as

$$I(\boldsymbol{\xi}) \approx \sum_{i=1}^{M}\sum_{j=1}^{N}\sum_{\omega}|f(\omega)|^2|\omega|^{-2}S^*_{ij}(\boldsymbol{\xi}|\omega)R_{ij}(\boldsymbol{\xi}|\omega), \tag{5}$$

or by defining $|f(\omega)|^2 = |\omega|^2$ we obtain

$$I(\boldsymbol{\xi}) \approx \sum_{i=1}^{M}\sum_{j=1}^{N}\sum_{\omega}S^*_{ij}(\boldsymbol{\xi}|\omega)R_{ij}(\boldsymbol{\xi}|\omega), \tag{6}$$

which demonstrates the equivalence between plane-wave and shot-profile migration (**?**).

Conical-wave migration

A second plane-wave migration formulation is to treat each 3D source plane-wave migration as if it were independent of the cross-line ray parameter. Note that this framework only is true in certain circumstances: straight sail lines and no flip-flop sources (**?**). Mathematically, this requires satisfying the condition that $j - l = 0$ in the exponential function in equation 3. If this relation holds, then we may write the following for the conical-wave image, I^{cw}_j, for the jth sail line:

$$\begin{aligned} I^{cw}_j(\boldsymbol{\xi}) &= \sum_{p_{\xi_1}} I_j(\boldsymbol{\xi}|p_{\xi_1}) \\ &= \sum_{p_{\xi_1}}\sum_{i,k=1}^{M}\sum_{\omega} S^*_{ij}(\boldsymbol{\xi}|\omega)R_{kj}(\boldsymbol{\xi}|\omega)|f(\omega)|^2 \mathrm{e}^{\mathrm{i}\omega p_{\xi_1}\Delta\xi_1(i-k)} \\ . &\approx \sum_{i=1}^{M}\sum_{\omega}|\omega|^{-1}|f(\omega)|^2 S^*_{ij}(\boldsymbol{\xi}|\omega)R_{ij}(\boldsymbol{\xi}|\omega), \end{aligned} \tag{7}$$

or, by defining $|f(\omega)|^2 = |\omega|$, we may rewrite

$$I^{cw}_j(\boldsymbol{\xi}) = \sum_{i=1}^{M}\sum_{\omega} S^*_{ij}(\boldsymbol{\xi}|\omega)R_{ij}(\boldsymbol{\xi}|\omega). \tag{8}$$

Stacking the individual sail-line conical-wave migration results yields the full image volume,

$$I(\boldsymbol{\xi}) = \sum_{j=1}^{N} I^{cw}_j(\boldsymbol{\xi}) = \sum_{j=1}^{N}\sum_{i=1}^{M}\sum_{\omega} S^*_{ij}(\boldsymbol{\xi}|\omega)R_{ij}(\boldsymbol{\xi}|\omega). \tag{9}$$

This completes the proof of the equivalence of conical-wave and shot-profile migration (**?**).

TILTED ELLIPTIC CYLINDRICAL COORDINATES

One question to be addressed is why did we choose TEC coordinates for conical-wave migration? We assert that the geometry of a TEC coordinate system, shown in figures 1 and 2, are well-suited to conical-wave migration. In particular, the width of the first extrapolation step allows us to position individual, as well as multiple, streamers of a single sail line directly on a single mesh. The singular points of the coordinate system also are located along the side edges, which facilitates numerical stability. We note that the other natural coordinate system, polar cylindrical coordinates, is not a judicious choice for conical-wave migration because the geometry: i) permits only single-streamer data to be placed on the mesh; and ii) has singular points located on the surface at the first extrapolation step.

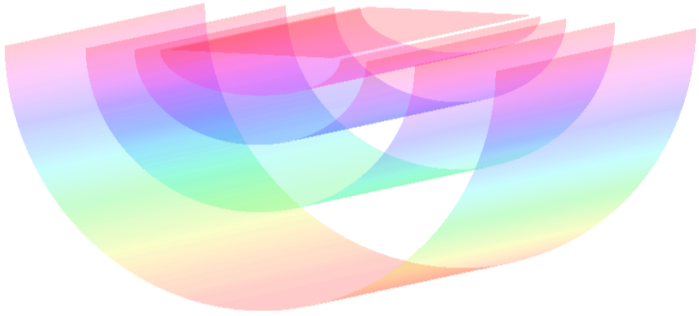

Figure 1: Four extrapolation steps in ξ_3 of an TEC coordinate system with a 0° tilt angle. The ξ_1 coordinate axis is oriented in the inline direction, while the ξ_2 coordinate axis is directed toward the crossline direction. [**NR**]

Figure 2: As in figure 1, but for a 25° tilt angle. [**NR**]

We begin by defining the transformation between the Cartesian and elliptic cylindrical meshes. We denote a Cartesian coordinate system by $\boldsymbol{x} = [x_1, x_2, x_3]$ and specify the tilted elliptic cylindrical mesh by $\boldsymbol{\xi} = [\xi_1, \xi_2, \xi_3]$. We set up our elliptic cylindrical geometry as follows:

- $\xi_1 \in [-\infty, \infty]$ is the inline direction, where surfaces of constant ξ_1 are 2D elliptic coordinate meshes;
- $\xi_2 \in [0, 2\pi)$ is the cross-line direction, where surfaces of constant ξ_2 are folded hyperbolic planes; and

- $\xi_3[0,\infty]$ is the extrapolation direction, where surfaces of constant ξ_3 form concentric elliptic cylinders.

The mapping relationship between the two coordinate systems is given by (**?**)

$$\begin{bmatrix} x_1 \\ x_2 \\ x_3 \end{bmatrix} = \begin{bmatrix} \xi_1 \cos\gamma - a \sinh\xi_3 \sin\xi_2 \sin\gamma \\ a \cosh\xi_3 \cos\xi_2 \cos\gamma \\ \xi_1 \sin\gamma + a \sinh\xi_3 \sin\xi_2 \cos\gamma \end{bmatrix}, \tag{10}$$

where γ is the inline tilt angle of the coordinate system and parameter a controls the coordinate system breadth. Figure 1 shows a TEC coordinate system for a 0° tilt angle, while figure 2 shows the same coordinate system, but for a 25° tilt angle.

TEC extrapolation wavenumber

The metric tensor ($g_{ij} = \frac{\partial x_k}{\partial \xi_i}\frac{\partial x_k}{\partial \xi_j}$ with an implicit summation over k) describing the geometry of the elliptic coordinate system is given by,

$$[g_{ij}] = \begin{bmatrix} 1 & 0 & 0 \\ 0 & A^2 & 0 \\ 0 & 0 & A^2 \end{bmatrix}, \tag{11}$$

where $A = a\sqrt{\sinh^2\xi_3 + \sin^2\xi_2}$. The determinant of the metric tensor is: $\sqrt{|\boldsymbol{g}|} = A^4$. The associated (inverse) metric tensor is given by,

$$\left[g^{ij}\right] = \begin{bmatrix} 1 & 0 & 0 \\ 0 & A^{-2} & 0 \\ 0 & 0 & A^{-2} \end{bmatrix}, \tag{12}$$

and weighted metric tensor ($m^{ij} = \sqrt{|\boldsymbol{g}|}\, g^{ij}$) is given by,

$$\left[m^{ij}\right] = \begin{bmatrix} A^2 & 0 & 0 \\ 0 & 1 & 0 \\ 0 & 0 & 1 \end{bmatrix}. \tag{13}$$

Note that even though the TEC coordinate system varies spatially, the local curvature parameters ($n^i = \frac{\partial m^{ij}}{\partial \xi_j}$) remain constant: $n^1 = n^2 = n^3 = 0$. The corresponding extrapolation wavenumber, k_{ξ_3}, can be generated by inputting tensors g^{ij}, m^{ij} and n^j into the general wavenumber expression for 3D non-orthogonal coordinate systems (**?**).

$$k_{\xi_3} = \pm\sqrt{A^2 s^2\omega^2 - k_{\xi_1}^2 - A^2 k_{\xi_2}^2}, \tag{14}$$

where s is the slowness (reciprocal of velocity).

The wavenumber developed in equation 14 is central to developing a shot-profile migration algorithm. This procedure consists of two parts. First, one extrapolates the source S_{ij} and receiver R_{kl} wavefields according to

$$S_{ij}(\xi_1,\xi_2,\xi_3+\Delta\xi_3|\omega) = \quad \mathbf{E}[S_{ij}(\xi_1,\xi_2,\xi_3|\omega)], \tag{15}$$
$$R_{kl}(\xi_1,\xi_2,\xi_3+\Delta\xi_3|\omega) = \quad \mathbf{E}[R_{kl}(k_{\xi_1},k_{\xi_2},\xi_3|\omega)], \tag{16}$$

where $\mathbf{E}[\cdot]$ is an extrapolation operator. The results in this paper were computed using frequency-space, $\omega-\mathbf{x}$, finite-difference extrapolators (see below).

The second step involves summing the individual shot images contributions, $I^{sp}_{ij}(\boldsymbol{\xi})$, into the total image volume, $I(\boldsymbol{\xi})$. Individual shot images are generated by correlating the S_{ij} and R_{kl} profiles:

$$I(\boldsymbol{\xi}) = \sum_{i=1}^{M}\sum_{j=1}^{N} I^{sp}_{ij}(\boldsymbol{\xi}) \tag{17}$$
$$= \sum_{i,k=1}^{M}\sum_{j,l=1}^{N}\sum_{\omega} S^{*}_{ij}(\boldsymbol{\xi}|\omega)R_{kl}(\boldsymbol{\xi}|\omega)\delta_{ik}\delta_{jl} \tag{18}$$

where symbol * denotes complex conjugation, M and N are the maximum number of inline and crossline sources, and $\delta_{ik}\delta_{jl}$ are delta functions forcing the source and receiver profiles to be from the same inline and cross-line shot location.

3D IMPLICIT FINITE-DIFFERENCE EXTRAPOLATION

A naturally arising concern is whether the dispersion relationship in equation 14 can be implemented accurately and efficiently in a wavefield extrapolation scheme. We address this question by comparing the elliptic cylindrical and the Cartesian elliptically anisotropic media dispersion relationships. By defining an effective slowness $s_A = As$ and rewriting equation 14 as

$$\frac{k_{\xi_3}}{\omega s_A} = \sqrt{1-\frac{k^2_{\xi_1}}{\omega^2 s^2_A} - A^2\frac{k^2_{\xi_2}}{\omega^2 s^2_A}}, \tag{19}$$

we observe that the TEC coordinate dispersion relationship resembles that for elliptically anisotropic media (**?**). More specifically, TEC coordinates relate to a special case where the Thomsen parameters (**?**) obey $\epsilon=\delta$

$$\left.\frac{k_{x_3}}{\omega s}\right|_{\epsilon=\delta} = \left.\sqrt{\frac{1-(1+2\epsilon)\frac{k^2_{x_1}+k^2_{x_2}}{\omega^2 s^2}}{1-2(\epsilon-\delta)\frac{k^2_{x_1}+k^2_{x_2}}{\omega^2 s^2}}}\right|_{\epsilon=\delta} = \sqrt{1-(1+2\epsilon)\frac{k^2_{x_1}}{\omega^2 s^2}-(1+2\epsilon)\frac{k^2_{x_2}}{\omega^2 s^2}}. \tag{20}$$

From equation 20 we see that equation 14 is no more complex than the dispersion relationship for propagating waves in elliptically anisotropic media, which is now routinely handled with optimized finite-difference approaches (**???**).

Rational Approximations

A general approach to 3D implicit finite-difference propagation is to approximate the square-root by a series of rational functions (**?**)

$$S_{\xi_3} = \sqrt{1 - S_{\xi_1}^2 - A^2 S_{\xi_2}^2} \approx \sum_{i=1}^{n} \frac{a_i S_r^2}{1 - b_i S_r^2}, \tag{21}$$

where $S_{\xi_i} = \frac{k_{\xi_i}}{\omega s_A}$ and $S_r^2 = S_{\xi_1}^2 + A^2 S_{\xi_2}^2$, for $i = 1, 2, 3$, and n is the order of the coefficient expansion. At this point, we do not address the anisotropy generated by the A coefficient, as it can be implemented through an additional slowness model stretch.

One procedure for finding an optimal set of coefficients is to solve the following optimization problem (**?**),

$$\min \int_0^{\sin\phi} \left[\sqrt{1 - S_r^2} - \sum_{i=1}^{n} \frac{a_i S_r^2}{1 - b_i S_r^2} \right]^2 \mathrm{d}S_r, \tag{22}$$

where ϕ is the maximum optimization angle. We generated the following results using a 4th-order approximation and coefficients found in Table 1 (Lee and Suh, 1985).

Extrapolation Algorithm

Using the 4th-order approximation is equivalent to solving a cascade of partial differential equations (**?**)

$$\begin{aligned}
\frac{\partial}{\partial \xi_3} U &= \mathrm{i}\omega s U, \\
\frac{\partial}{\partial \xi_3} U &= \mathrm{i}\omega s \left[\frac{\frac{a_1}{\omega^2 s_A^2} \frac{\partial^2}{\partial \xi_1^2}}{1 + \frac{b_1}{\omega^2 s_A^2} \frac{\partial^2}{\partial \xi_1^2}} + \frac{\frac{a_1}{\omega^2 s^2} \frac{\partial^2}{\partial \xi_2^2}}{1 + \frac{b_1}{\omega^2 s^2} \frac{\partial^2}{\partial \xi_2^2}} \right] U, \\
\frac{\partial}{\partial \xi_3} U &= \mathrm{i}\omega s \left[\frac{\frac{a_2}{\omega^2 s_A^2} \frac{\partial^2}{\partial \xi_1^2}}{1 + \frac{b_2}{\omega^2 s_A^2} \frac{\partial^2}{\partial \xi_1^2}} + \frac{\frac{a_2}{\omega^2 s^2} \frac{\partial^2}{\partial \xi_2^2}}{1 + \frac{b_2}{\omega^2 s^2} \frac{\partial^2}{\partial \xi_2^2}} \right] U.
\end{aligned} \tag{23}$$

We solve these equations implicitly at each extrapolation step by a finite-difference splitting method that alternatively advances the wavefield in the ξ_1 and ξ_2 directions. Splitting methods allow us to apply the A scaling factor directly by introducing the original slowness model: $\frac{s_A}{A} = s$.

One drawback to splitting methods is that they generate numerical anisotropy. To minimize these effects, we apply a Fourier-domain phase-correction filter (**?**)

$$U = U \mathrm{e}^{\mathrm{i}\Delta\xi_3 k_L}, \tag{24}$$

Coeff. order i	Coeff. a_i	Coeff. b_i
1	0.040315157	0.873981642
2	0.457289566	0.222691983

Table 1: Coefficients used in 3D implicit finite-difference wavefield extrapolation.

where

$$k_L = \sqrt{1 - \frac{k_{\xi_1}^2}{(\omega s_1^r)^2} - \frac{k_{\xi_2}^2}{(\omega s_2^r)^2}} - \left[1 - \sum_{i=1}^{2} \left(\frac{a_i (\frac{k_{\xi_1}}{\omega s_A^r})^2}{1 - b_i (\frac{k_{\xi_1}}{\omega s_A^r})^2} - \frac{a_i (\frac{k_{\xi_2}}{\omega s_A^r})^2}{1 - b_i (\frac{k_{\xi_2}}{\omega s_A^r})^2} \right) \right], \quad (25)$$

and s_1^r and s_2^r are reference slownesses chosen to be the mean value of s_{eff}^A and s defined above.

NUMERICAL TESTS

We conducted impulse response tests on a 500 x 400 x 400 mesh in a homogeneous medium with slowness $s = 0.0005$ s/m. The initial wavefield consisted of three smoothed point sources at $t = [0.5, 0.75, 1]$ s. Using this experimental setup, we expect the impulse responses to consist of three hemispherical surfaces of radii $r = [1000, 1500, 2000]$ m.

Figure 3 shows the inline and crossline responses in the upper and lower panels, respectively. To illustrate the accuracy of the approach, we overlaid three lines showing that the analytical answers. Note that the impulse responses are limited at high angles both by the coordinate system boundaries and by the 50 sample cosine-taper function applied at the edges. Figure 4 shows the 1300m depth slice. The symmetric response indicates that the numerical anisotropy from the numerical splitting has been accounted for by the Li phase-correction filter.

CONCLUSIONS

This paper introduces the tilted elliptic cylindrical coordinate system to conical-wave migration. We demonstrate that corresponding extrapolation wavenumber is no more complicated than that of elliptically anisotropic media. This allows us to implement an accurate finite-difference extrapolation approach that can handle the effective anisotropy. Future work will apply the algorithm to 3D data.

ACKNOWLEDGMENTS

We would like to thank Ben Witten for helpful conversations.

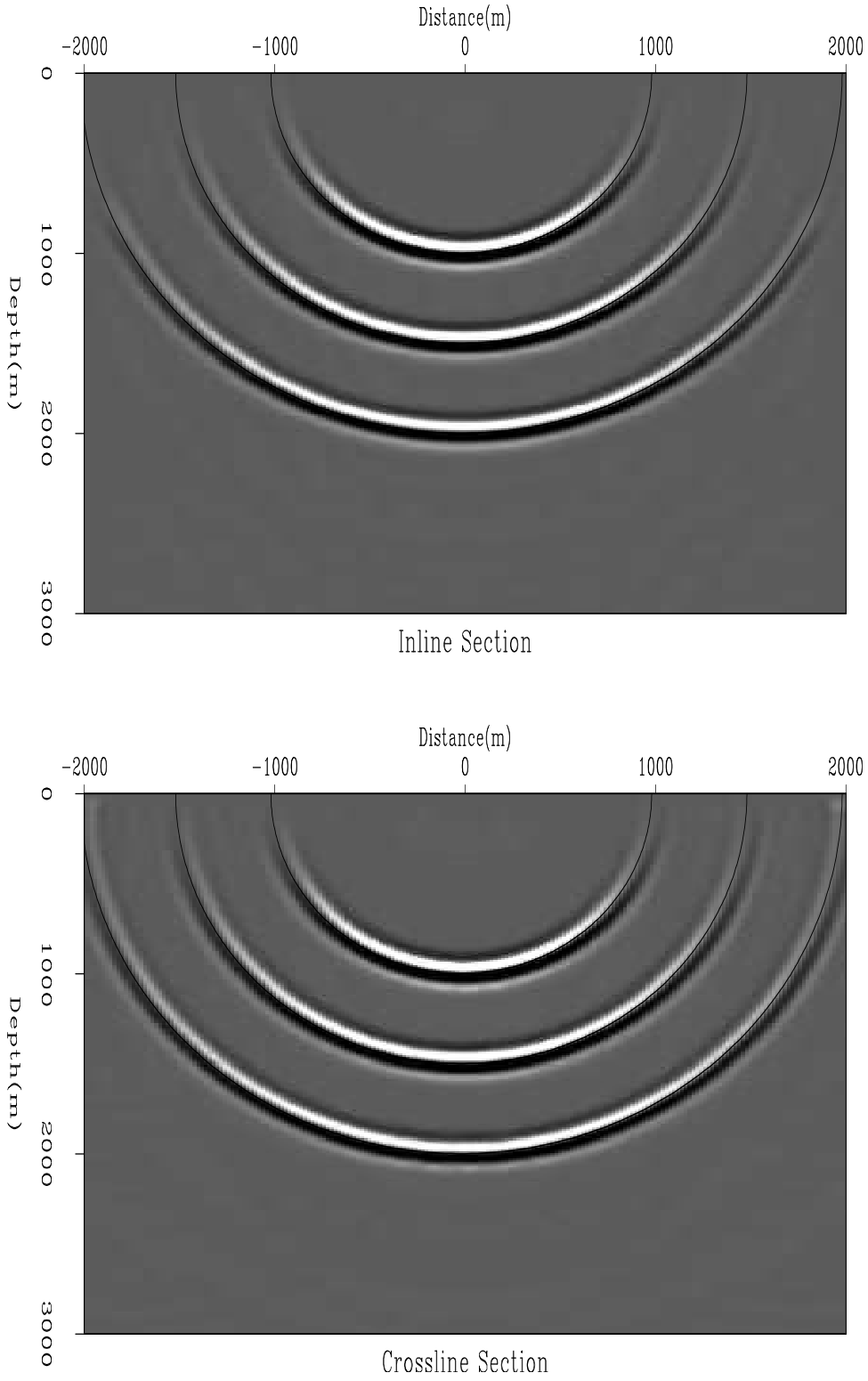

Figure 3: Elliptic cylindrical coordinate impulse response cross sections through the 3D image volume. Top panel: Inline response. Bottom panel: Crossline response.[**CR**]

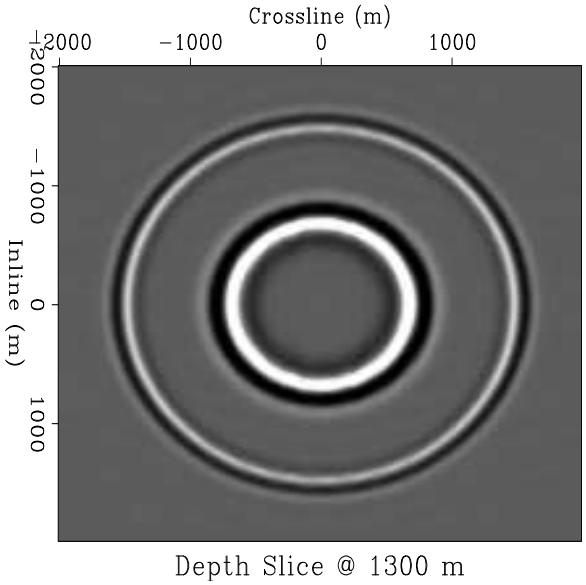

Figure 4: Image volume depth slice taken at 1300m. Note the circular symmetry of the impulse response. [**CR**]

REFERENCES

Lee, M. W. and S. Y. Suh, 1985, Optimization of one-way wave-equations (short note): Geophysics, **50**, 1634–1637.